

## Experimental evaluation of aerodynamic damping of square super high-rise buildings

Yong Quan<sup>†</sup> and Ming Gu<sup>‡</sup>

State Key Laboratory Disaster Reduction in Civil Engineering, Tongji University, 1239, Siping Road, Shanghai, 200092, China

Yukio Tamura<sup>‡†</sup>

Department of Architecture, Tokyo Polytechnic University, 1583, Iiyama, Atsugi, Kanagawa, 243-0297, Japan  
(Received October 14, 2004, Accepted January 20, 2005)

**Abstract.** Aerodynamic damping often plays an important role in estimations of wind induced dynamic responses of super high-rise buildings. Across- and along-wind aerodynamic damping ratios of a square super high-rise building with a height of 300 m are identified with the Random Decrement technique (RDT) from random vibration responses of the SDOF aeroelastic model in simulated wind fields. Parametric studies on effects of reduced wind velocity, terrain type and structural damping ratio on the aerodynamic damping ratios are further performed. Finally formulas of across- and along-wind aerodynamic damping ratios of the square super high-rise building are derived with curve fitting technique and accuracy of the formulas is verified.

**Keywords:** super high-rise building; aerodynamic damping; wind induced response; aeroelastic model wind tunnel test.

### 1. Introduction

By comparing buildings' responses calculated in terms of pressure distributions obtained from wind tunnel tests of their rigid models with those from aeroelastic model tests, Kareem (1978) pointed out that the effect of aerodynamic damping on wind induced vibration of high-rise buildings is not always negligible. Sometimes, across-wind aerodynamic damping of buildings appears negative value, which will increase building vibration amplitude.

Since aerodynamic damping sometimes plays an important role in wind excited dynamic responses of high-rise buildings and structures, after the Kareem's research, a number of studies on aerodynamic damping have been performed. Steckley (1989) developed a pivot mode activator system to measure motion-induced forces on aeroelastic models of high-rise structures to obtain the aerodynamic impedances of prisms. Based on Steckley's experiments, Watanabe, *et al.* (1997) proposed a fitted empirical aerodynamic damping function. Using the Random Decrement technique

---

<sup>†</sup> COE Researcher, Currently, Tokyo Polytechnic University, E-mail: [quanyong@arch.t-kougei.ac.jp](mailto:quanyong@arch.t-kougei.ac.jp)

<sup>‡</sup> Professor, E-mail: [minggu@mail.tongji.edu.cn](mailto:minggu@mail.tongji.edu.cn)

<sup>‡†</sup> Professor, E-mail: [yukio@arch.t-kougei.ac.jp](mailto:yukio@arch.t-kougei.ac.jp)

(RDT) to deal with random vibration data of aeroelastic models under simulated wind fields in a wind tunnel, Marukawa, *et al.* (1996) investigated aerodynamic damping characteristics of square and rectangle high-rise buildings. Nishimura and Taniike (1995), Glanville, *et al.* (1996) and some other researchers have studied aerodynamic damping too.

Aerodynamic damping usually depends on reduced wind velocity and vibration amplitude influenced by mass ratio and structural damping or the Scruton Number. In this paper, a study on along- and across-wind aerodynamic damping ratios of a typical square super high-rise building with different structural damping ratios in different wind fields is carried out through a series of wind tunnel tests on the SDOF aeroelastic model to investigate the effects of the parameters on the aerodynamic damping. Finally formulas of across- and along-wind aerodynamic damping ratios of such buildings are derived with curve fitting technique.

## 2. Outline of the wind tunnel test

### 2.1. Simulations of wind characteristics

The test was carried out in TJ-1 Boundary Layer Wind Tunnel, whose working section is 1.8 m in width and 1.8 m in height, and the wind speed ranges from 3 to 32 m/s. Four kinds of wind conditions, corresponding to terrain categories A, B, C and D, were simulated in the wind tunnel at a length scale of 1/500 in accordance with the Chinese load code (2001). The exponents of the mean wind profiles for the terrain categories A, B, C and D are 0.12, 0.16, 0.22 and 0.30, and the corresponding gradient heights are 300, 350, 400 and 450 m, respectively. The wind characteristics are achieved by a combination of turbulence generating spires, a barrier at the entrance of the wind tunnel, and roughness elements along the wind tunnel floor upstream of the model. Fig. 1 shows the simulated mean wind speed profiles, the longitudinal and lateral component profiles of turbulence intensities and the power spectra of longitudinal fluctuating wind speeds for the terrain categories B and D. The longitudinal turbulence intensities at the height of 300 m (0.6 m in the wind tunnel) are about 6.8%, 7.3%, 10% and 14% for the four categories of terrain, respectively; and the lateral turbulence intensities at the same height are somewhat lower than the corresponding longitudinal components.

### 2.2. Building model

The building model has a height of 60 cm, representing a height of 300 m for the real building. In order to make a reasonable investigation of effects of factors on the aerodynamic damping, the structural parameters of the typical super high-rise building should be first determined.

Tamura (2000) suggested an Eq. (1) to estimate the 1st translation mode natural period of common high-rise buildings in terms of investigations of a great number of tall buildings in Japan.

$$T_1 = \begin{cases} 0.015H : RC \text{ \& } SRC \text{ Building (small-amplitude)} \\ 0.020H : Steel \text{ Building (small-amplitude)} \end{cases} \quad (1)$$

Thus the first mode frequency of high-rise buildings with a height of 300 m should be

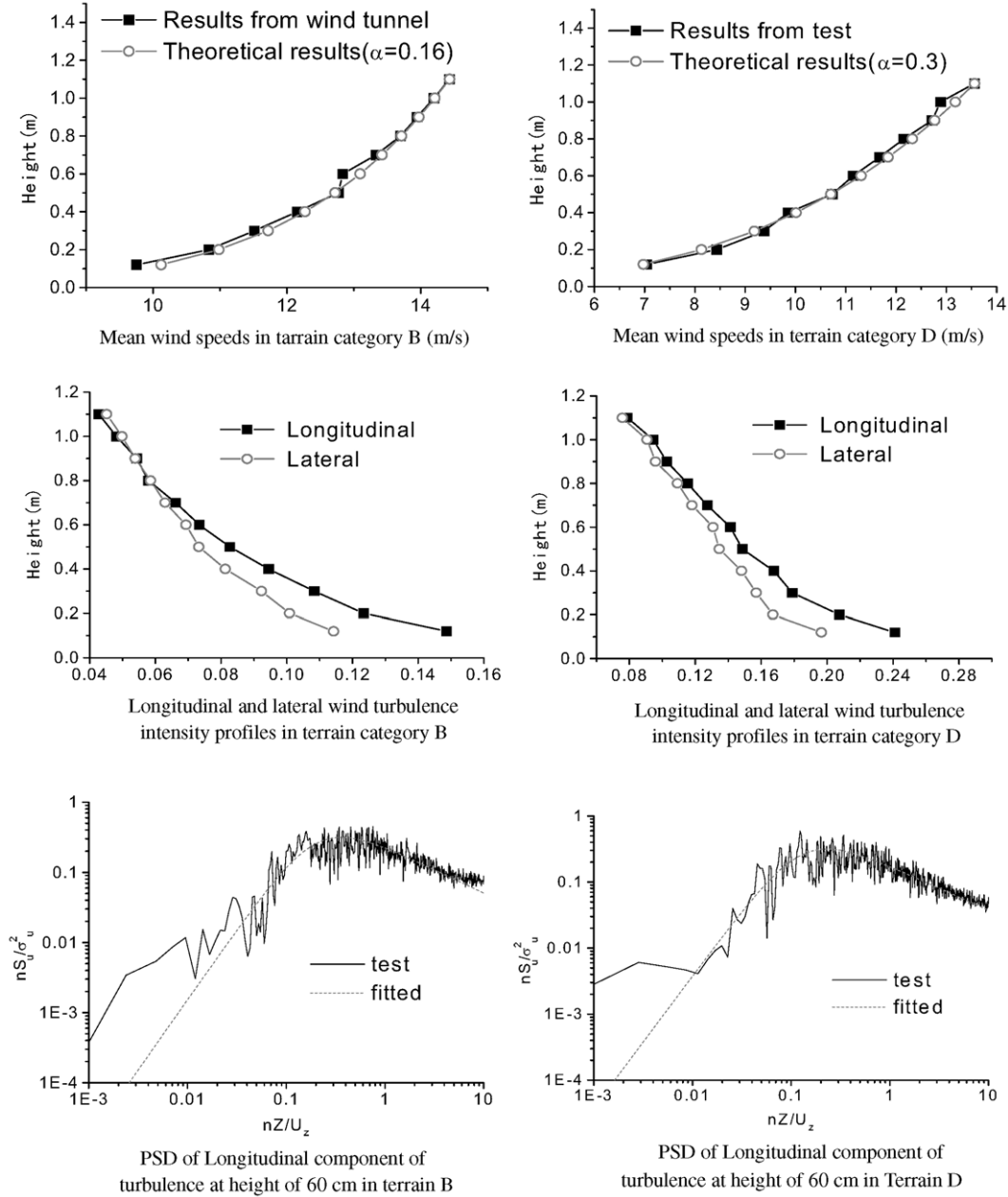


Fig. 1 Simulated wind parameters of the terrain categories B and D

$$f_1 = 1/T_1 = 1/(0.015H \sim 0.02H) = 0.167 \sim 0.222 \text{ Hz} \quad (2)$$

In the present research, the first frequency is determined to be 0.19 Hz.

In addition, average mass densities of common high-rise buildings usually are 160~240 kg/m<sup>3</sup>. Since super high-rise buildings are prone to light, the mass density of the typical building is set as 180 kg/m<sup>3</sup>.

The wind velocity scale of the wind tunnel test is set as 1/8. Correspondingly, other scales, such as structural mass scale, frequency scale, etc., are determined in terms of above basic scales,  $C_V$  and  $C_L$ . Thus the mass and frequency and time scales are, respectively,  $C_m = 1.25 \times 10^8$ ,  $C_f = 62.5$  and  $C_t = 1/62.5$ .

For design of the SDOF aeroelastic model, generalized structural parameters, e.g., generalized mass and generalized stiffness, are further determined in terms of its physical parameters. The first bending mode shape function of the model is assumed to be  $\varphi(z) = z/H$ . Thus the generalized mass and the generalized stiffness of the model can be calculated using Eq. (3) and Eq. (4), respectively.

$$M = \int_0^H m(z) \times \varphi^2(z) dz \quad (3)$$

$$K = 4\pi^2 f^2 M = \sum_{i=1}^n k_i \times (l_i / H)^2 \quad (4)$$

in which,  $H$  is the height of model;  $m(z)$  is the mass per unit length of the model;  $n$  is the number of springs installed on the elastically supporting base of model system shown in Fig. 2;  $k_i$  is the stiffness of the  $i$ th spring;  $l_i$  is the distance between the  $i$ th spring and the rotating center of the base.

Finally the generalized mass and the generalized stiffness of the aeroelastic model are determined, respectively, to be  $M = 0.36$  kg and  $K = 2.01 \times 10^3$  kg/s<sup>2</sup> in accordance with full-scale building mass density of 180 kg/m<sup>3</sup> and first mode frequency of 0.19 hz. In addition, four kinds of structural damping ratios are adopted in the test, which are  $\zeta_s = 0.6\%$ , 1.2%, 1.88% and 2.17%.

Fig. 2 shows the specially designed supporting base of the aeroelastic model, on which the rigid building model can vibrate in two perpendicular directions under wind actions. The required first-mode generalized mass and stiffness can be achieved respectively by selecting proper mass blocks and springs according to Eq. (3) and Eq. (4). And the structural damping ratios can be simulated through selecting proper size of the damping cards and their depth immersed into an oil pool. In the

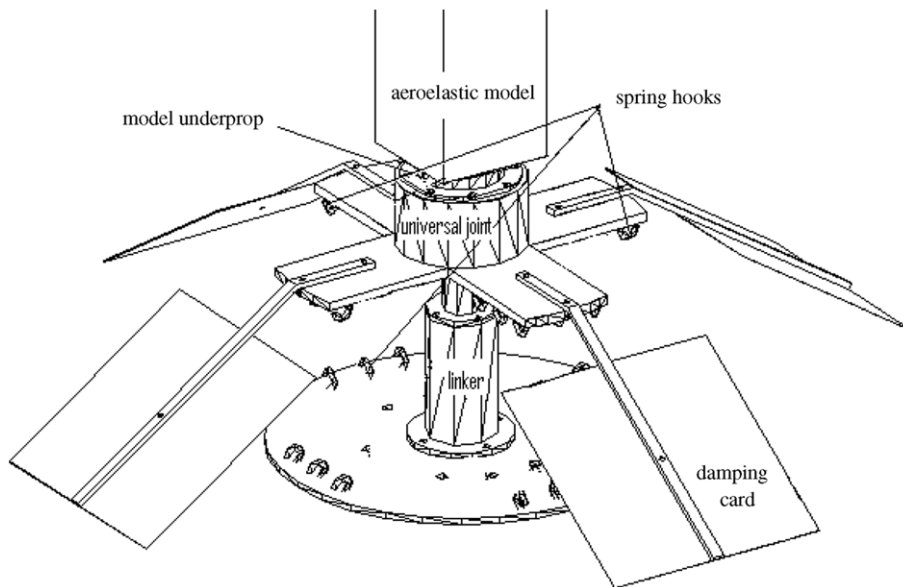


Fig. 2 Base of the SDOF aeroelastic model

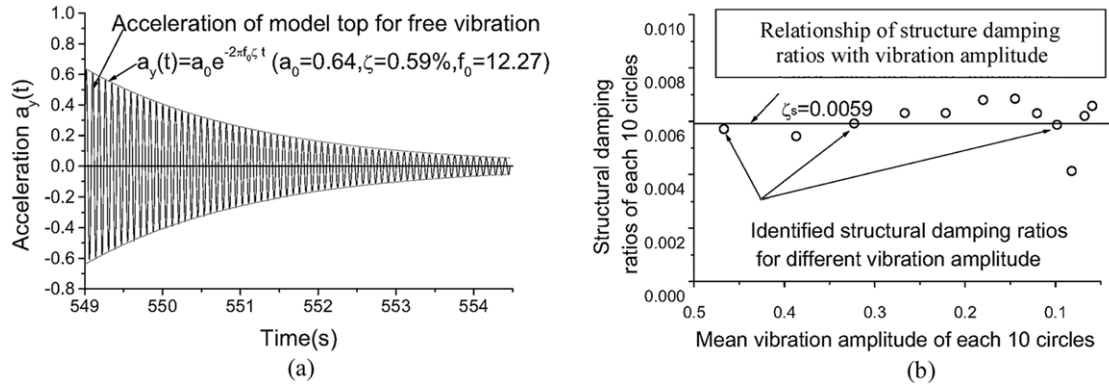


Fig. 3 A free vibration signature of a testing model case and structural damping ratios for different vibration amplitudes

wind tunnel test, the damping cards are bended to their vibration direction in oil pool to make the structural damping ratios independent of their vibration amplitudes. Two mini-accelerometers are perpendicularly mounted on the top of the model to measure across- and along-wind responses respectively. The testing wind velocity at the level of model height ranges from 4 m/s to 16 m/s, with the increment of 1 m/s in non-vortex-excitation zones and of 0.5 m/s in vortex-excitation zone.

Before the wind tunnel test, whether the structural damping is stable, i.e., un-variable with vibration amplitude of the building model, should be first checked. Fig. 3(a) shows a curve of free decay response of the model and Fig. 3(b) presents the identified damping ratios from different sections of the free decay response with different vibration amplitudes. From Fig. 3(b) one can see that the identified structural damping ratios are almost the same for different vibration amplitudes, which indicates that the identified structural damping ratio of the testing model doesn't vary with the vibration amplitude.

### 3. The method for identifying aerodynamic damping - the random decrement technique

The methods for estimating damping from a time history of random vibration response can be classified into two categories: spectral and time-series approaches. The spectral approaches are those related to spectral analysis, i.e., auto-correlation decay, spectra based half-power method and spectral moment method, etc. The time-series approaches include the Random Decrement technique (RDT), the maximum entropy estimates, the auto-regressive (AR), the moving averages (ARMA), and so on. Among these methods, RDT has been verified to be a desirable one to evaluate aerodynamic damping ratios from random vibration responses of structures excited by random wind loads. Jeary, *et al.* (1996), Tamura, *et al.* (1996), Kareem, *et al.* (1996) and some other papers have adopted this method for the purpose of identifying aerodynamic damping of tall buildings.

In the RDT, the total response of a dynamic system is regarded as a superposition of responses due to initial displacement, initial velocity and the random load input respectively as following:

$$x_T = x_{x0} + x_{\dot{x}0} + x_F \tag{5}$$

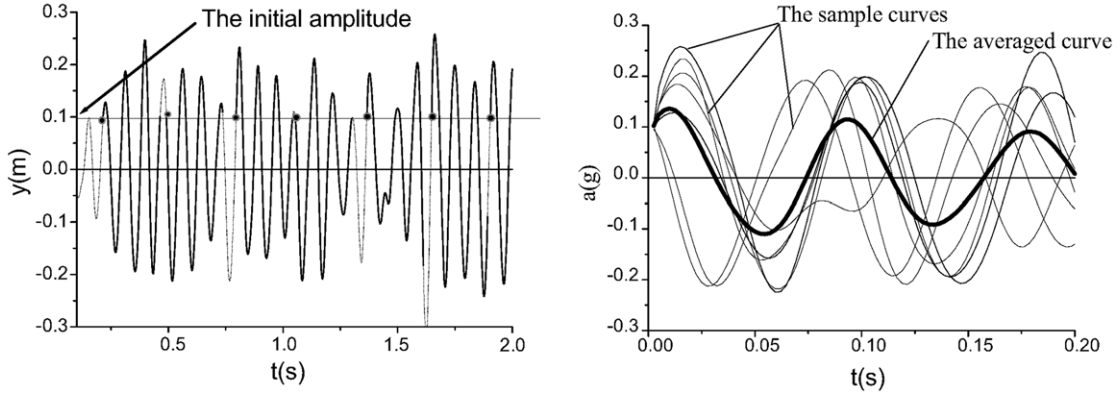


Fig. 4 The sketch of the process of the RDT

in which,  $x_T$  is the total displacement;  $x_{x_0}$  is the displacement component induced by the initial displacement;  $x_{\dot{x}_0}$  is the displacement component induced by the initial velocity;  $x_F$  is the displacement component induced by the random load.

Vibration response of a linear system due to a zero mean stationary random load input is also a zero mean random stationary. When the number of segments is very large, the ensemble average of such process tends to zero. Since all segments start at the same threshold level  $x_{th}$  and other original condition is random, the response due to random initial velocity and zero mean random load are averaged out. As a result, a free vibration due to initial displacement excitation at  $x_{th}$  remains :

$$\left( \sum_{n \rightarrow \infty} x_T \right) / n = \left( \sum_{n \rightarrow \infty} x_{x_0 = x_{th}} + \sum_{n \rightarrow \infty} x_{\dot{x}_0} + \sum_{n \rightarrow \infty} x_F \right) / n = x_{x_0 = x_{th}} + 0 + 0 = x_{x_0 = x_{th}} \quad (6)$$

Fig. 4 shows the basic process of the RDT.

In the present study, before the identification procedure, acceleration signals of the testing model are filtered at a filtering frequency range of  $(1 - 25\%)f_0 \leq f \leq (1 + 25\%)f_0$ , where  $f_0$  is natural frequency of the model. The threshold value of each segment,  $x_I$ , meets the requirements as :

$$abs(abs(x_I) - a) / a \leq 5\%. \text{ and } abs(abs(x_I) - a) \leq abs(abs(x_{I+j}) - a) \quad (7)$$

$$j = -10, -9, \dots, 9, 10$$

in which,  $a$  is the initial amplitude for the identification, which is taken as RMS value of the model response displacement in the present study since it is the reasonable represent of the random amplitude of model excited by random wind loads.

In the identification process, there are 7500~10000 segments to be averaged. Fig. 5 shows one of the RD signatures obtained from the wind tunnel test data, in which  $a$  is the initial amplitude for the identification and  $y$  is the instantaneous vibration displacement.

From the RD signature, the damping ratio of the dynamic system can be identified. When dynamic response of a structure system is induced by random wind load, the damping ratio identified with this method includes not only structural damping ratio but also aerodynamic damping ratio. After the structural damping ratio is subtracted from the total damping ratio, the aerodynamic damping ratios can be obtained.

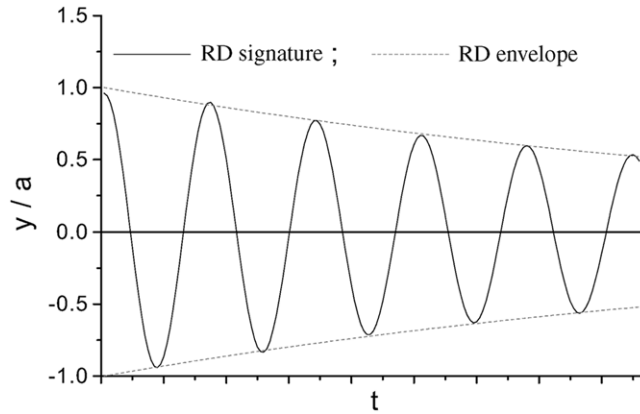


Fig. 5 One case of the RD signatures

#### 4. Identified results and comparison with others

Fig. 6 shows the identified aerodynamic damping ratios of the model and the comparison with aerodynamic damping ratios from other two literatures. Steckley (1989) studied across-wind aerodynamic damping using forced vibration technique. The exponent of mean wind profile was 0.115 and the turbulence intensity at the model top was 9% for the test. The reduced vibration amplitude (vibration amplitude of model top/ model width) was fixed at 3.2%. Marukawa, *et al.* (1996) identified along- and across-wind aerodynamic damping ratios using the RDT from a SDOF aeroelastic model wind tunnel test. The model was a square prism with an aspect ratio of 6. The exponent of the wind profile and the turbulent intensity at the top of the model were 0.167 and 10.7%, respectively; and the structural damping ratio of the building model was 1%. From Fig. 6, it can be seen that the across-wind aerodynamic damping ratios from the present test are close to those from Marukawa, but different from those of Steckley, especially at reduced wind velocity larger than 10, i.e., the vortex-excitation velocity range. The difference may be due to the difference between the vibration amplitudes. In Steckley's test, the forced vibration technique was adopted and

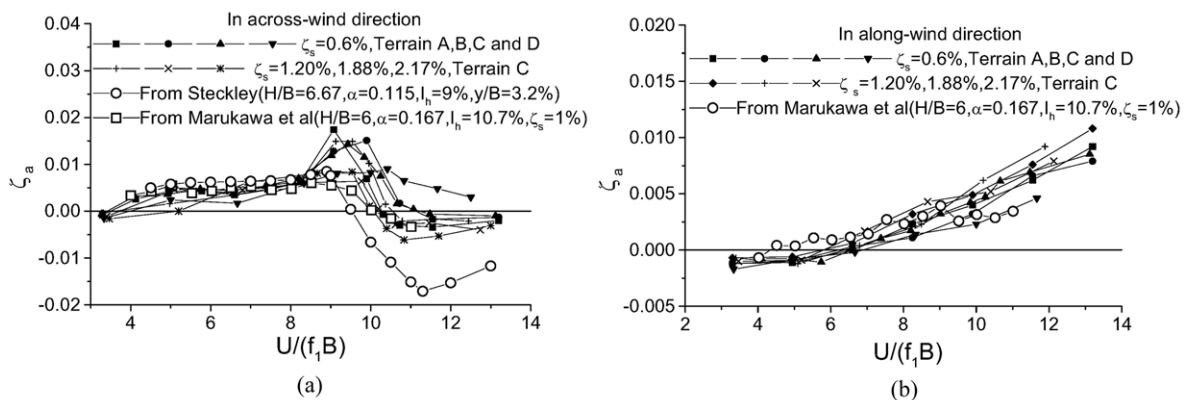


Fig. 6 Comparison of aerodynamic damping ratios from present study with that from literature

the reduced vibration amplitude was fixed at 3.2% while those in present test were changeable with reduced wind velocity. At low reduced wind velocities, since the difference of the reduced amplitude is not very large between Steckley test and present one (comparing with the test data for structural damping ratio of 2.17% and terrain C), the difference of the aerodynamic damping ratios from these two tests is small too. But when reduced wind velocity is large than 9, the reduced amplitudes in present test are large than those of Steckley's, which may lead to large differences between the aerodynamic damping ratios from the present study and Steckley's study.

In along-wind direction, aerodynamic damping ratios from the present test agree well with those from Marukawa.

## 5. The effects of parameters on aerodynamic damping ratio

The effects of reduced wind velocity, structural damping ratio and wind field type on across- and along- wind aerodynamic damping ratios are investigated.

### 5.1. Effect of reduced wind velocity

Fig. 7 shows variations of across- and along-wind aerodynamic damping ratios of the model with reduced wind velocity for the different test cases, i.e., different terrain condition and different structural damping. Although the values of the across- and along-wind damping ratios are different for different test cases, their variable tendencies with reduced velocity are similar each other. In across-wind direction, each curve of the aerodynamic damping ratios with the reduced wind velocity has a single peak. For the reduced wind velocity of about 3, the aerodynamic damping ratios are very small for most of the test cases. With the further increase of reduced wind velocity from 3, the aerodynamic damping ratios increase. When the reduced wind velocity arrives at 9 or 10, the aerodynamic damping ratios arrive at their maximum positive values. After that, with further increase of the reduced wind velocity, the aerodynamic damping ratios suddenly decrease; and when reduced wind velocity reaches 10 or 11, the aerodynamic damping ratios arrive at negative valleys for most of the test cases.

In along-wind direction, the aerodynamic damping ratios vary with reduced velocity nearly in a linear way. When the reduced wind velocity is less than 6, the aerodynamic damping ratios for majority of the test cases are negative, with very small absolute values. When reduce wind velocity increase, the aerodynamic damping ratios increase monotonously. When reduced wind velocity reaches to 10, the aerodynamic damping ratios will reach to about 0.5%.

### 5.2. Effect of terrain type

The testing results show that turbulence intensities for different categories of terrain will affect the vibration amplitude of the structure and consequently affect the aerodynamic damping. Fig. 8 presents the variations of the across-wind aerodynamic damping ratios for different terrain conditions. As can be seen, in the four types of terrains, positive peak of the aerodynamic damping curve for the terrain category A has a highest positive peak at the reduced frequency of about 9 and has a smallest negative valley at the reduced frequency about 11.5. The curve for the terrain category D has also a positive peak, but is much lower than those for the other categories of terrains, and has no negative damping for all the reduced velocities. In addition, the reduced wind velocity corresponding to the positive peak for the terrain category A is lowest while that for the

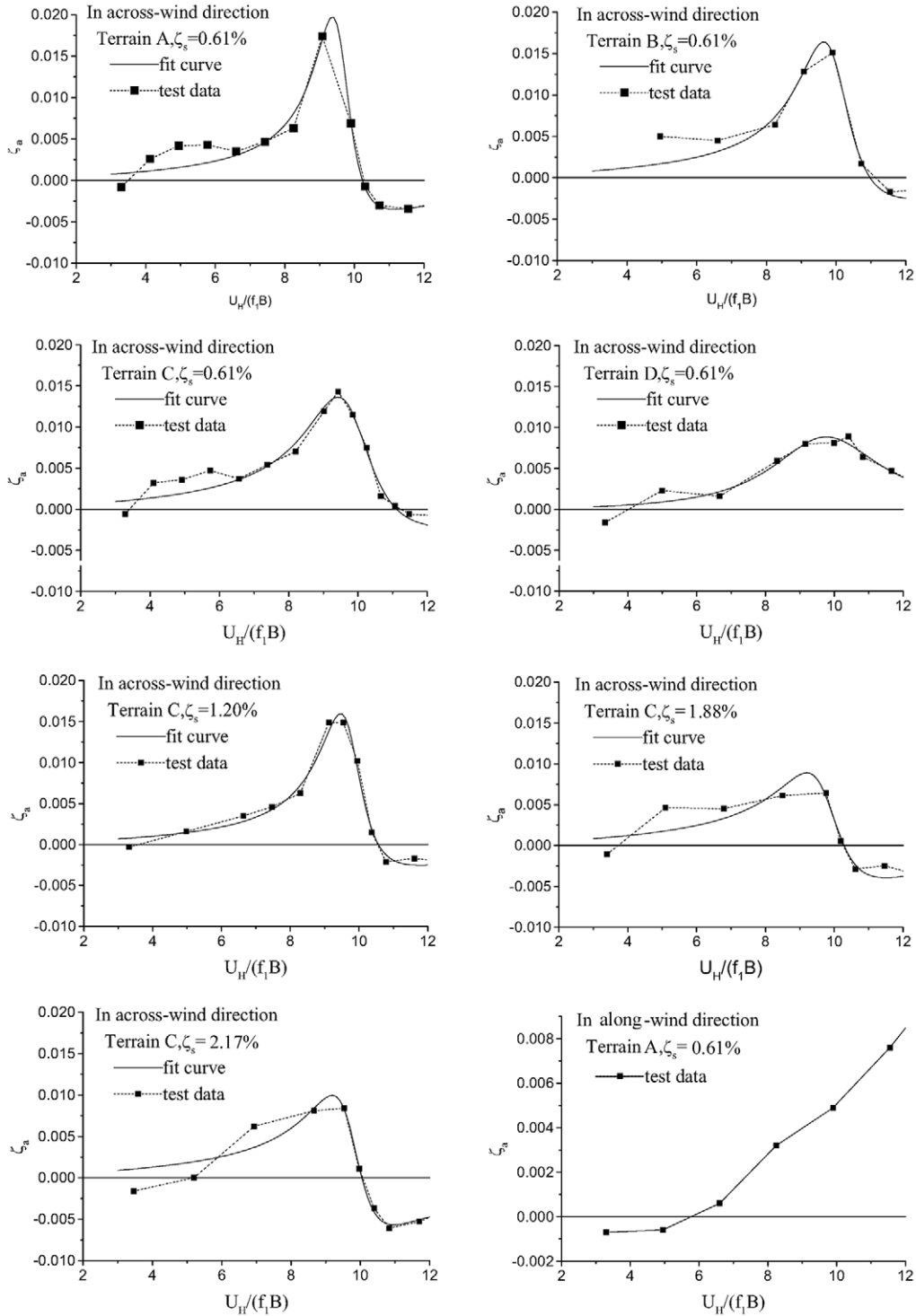


Fig. 7 Across- and along-wind aerodynamic damping ratios of the model in different test cases

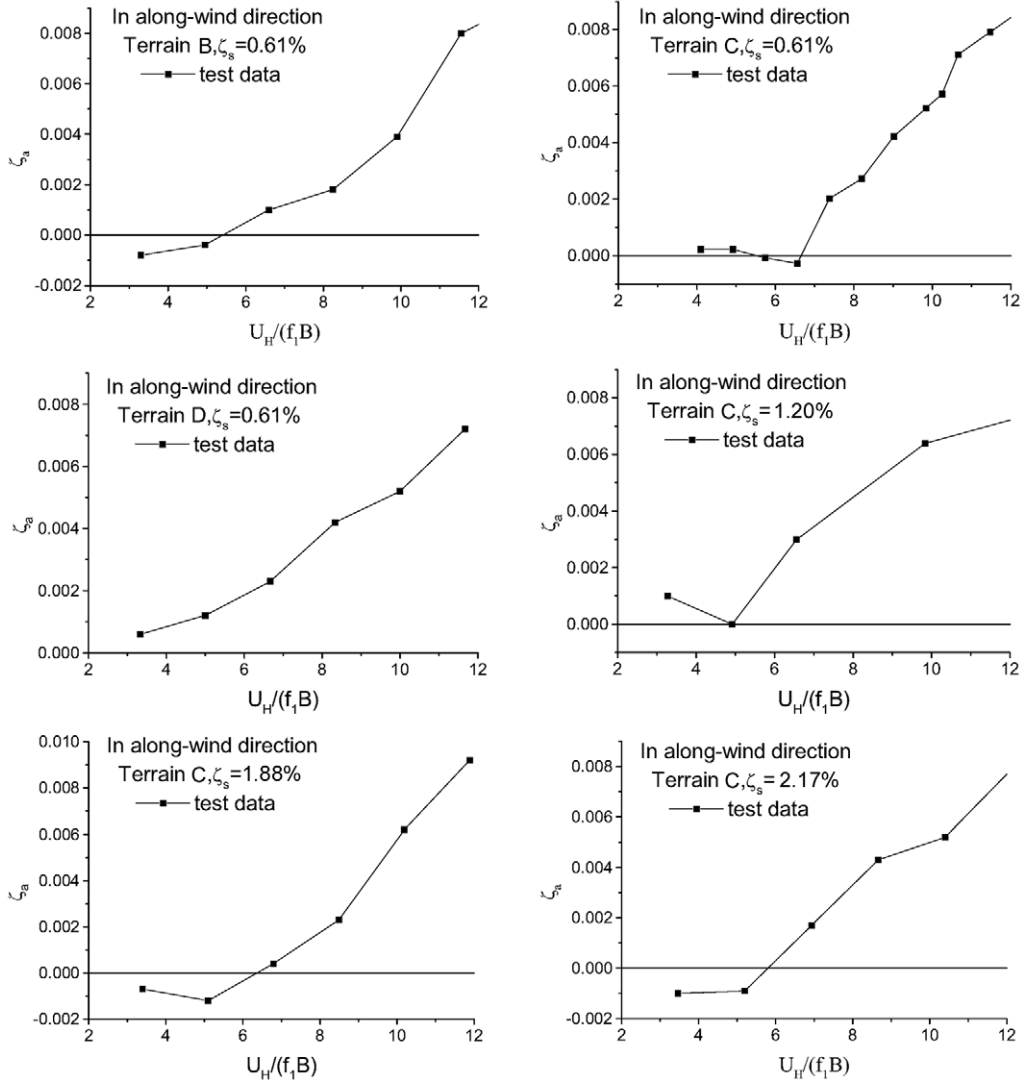


Fig. 7 Continued

terrain D is highest.

In Fig. 8(b), one can find that the across-wind aerodynamic damping ratios are almost the same for the four kinds wind conditions at low reduced wind velocities. For the reduced wind velocity of about 9, the across-wind aerodynamic damping ratios decrease with the increase of the sequence number of the terrains. For high reduced wind velocity, such as 11.5, they become negative for terrain categories A, B and C, and increase with the increase of sequence number of the terrains.

Fig. 9 presents the variation of along-wind aerodynamic damping ratios for different wind field conditions. From the figure one can find that the along-wind aerodynamic damping ratios for the four categories of terrain are almost the same and they increase with the reduced wind velocity approximately in a linear way.

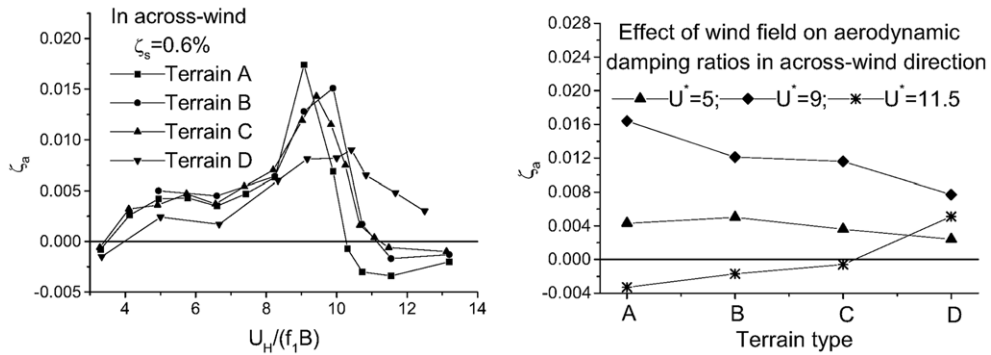


Fig. 8 Variations of across-wind aerodynamic damping ratio with different terrain conditions

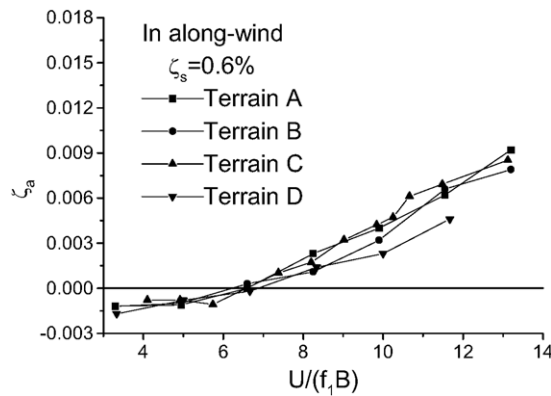


Fig. 9 Variation of along-wind aerodynamic damping ratios with different terrain conditions

### 5.3. Effect of structural damping ratio

Structural damping will affect vibration amplitudes of structures and consequently affect the aerodynamic damping. Fig. 10 shows the effect of structural damping ratio on the across-wind

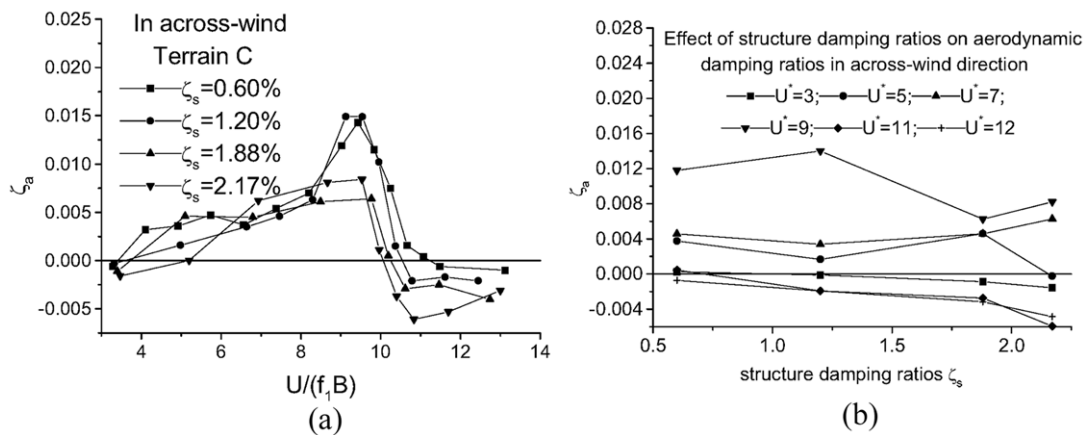


Fig. 10 Variation of across-wind aerodynamic damping ratio with different structural damping ratios

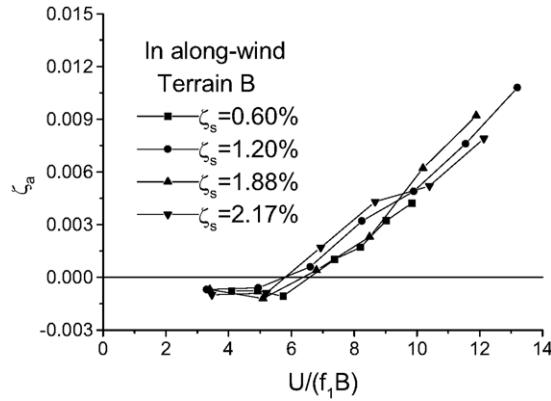


Fig. 11 Variations of along-wind aerodynamic damping ratio with different structural damping ratios

aerodynamic damping. For very low reduced wind velocities, such as 3, and high reduced wind velocities, such as 11 and 12, the across-wind aerodynamic damping ratios are negative and decrease with the increase of structural damping ratio; while for the other reduced wind velocities, such as 5 and 7 and 9, the across-wind aerodynamic damping ratios are positive but no obvious variation trend for different structural damping ratios.

Fig. 11 shows the along-wind aerodynamic damping ratio for buildings with different structural damping ratios. There is no obvious difference among them.

### 6. Fitted equations of aerodynamic damping ratios

From Fig. 7, it can be found that all of the curves of across-wind aerodynamic damping ratios versus reduced wind velocity are single peak curves. The following formula transformed from the frequency response function can be used to fit such curves:

$$\zeta_a = \frac{K_1(1 - r^2)r + K_2r^2}{(1 - r^2)^2 + \beta^2r^2} \tag{8}$$

in which,  $r$  is a independent variable, corresponding to reduced wind velocity, and will be discussed below;  $K_1$ ,  $K_2$  and  $\beta$  are parameters to be fitted. Fig. 12 shows the effects of these parameters on the configuration of one-peak curve, similar to the curve of the across-wind aerodynamic damping

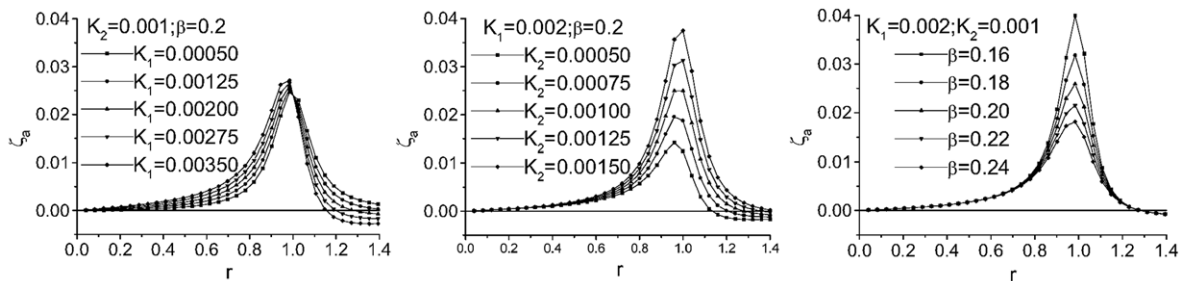


Fig. 12 Effect of parameters on Eq. (8)

Table 1 Parameters in Eq. (8)

Terrain	$\zeta_s$	$K_1$	$K_2$	$\beta$	$U_s$
A	0.006	0.00207	0.000256	0.125	9.62
B	0.006	0.00231	0.000435	0.177	9.99
C	0.006	0.00254	0.000603	0.230	9.87
D	0.006	0.00472	0.001381	0.396	9.90
C	0.012	0.00192	0.000306	0.151	9.75
C	0.019	0.00244	0.000211	0.206	9.85
C	0.022	0.00257	0.000124	0.171	9.80

curve.

From Fig. 12, one can find that the deflection of the curve is determined by the parameter  $K_1$ . When  $K_1$  increases, the curve values at the left side of the peak increase while those at right side decrease. The height of the peak is determined by parameter  $K_2$  and parameter  $\beta$ . When  $K_2$  increases or  $\beta$  decreases, the height of the peak increases. The bandwidth of the peak is determined by parameter  $\beta$ . When  $\beta$  increases, the bandwidth of the peak increases. Most of the single peak curves in Fig. 7 can be fitted according to the three parameters.

In Eq. (8),  $r = U^*/U_s$ , where  $U^* = U_H/(f_1B)$  is reduced wind velocity at the model height;  $K_1$ ,  $K_2$ ,  $U_s$  and  $\beta$  are derived with the test data using curve fitting technique and are listed in Table 1.  $U_s$  can be looked as reduced wind velocity corresponding to the peak of the aerodynamic damping ratio. Comparisons of the test results and Eq. (8) can also be found from Fig. 7.

For practical purpose, a simplified formula for the across-wind aerodynamic damping ratio can be further derived as

$$\zeta_a = \frac{0.0025(1 - (U^*/9.8)^2)(U^*/9.8) + 0.000125(U^*/9.8)^2}{(1 - (U^*/9.8)^2)^2 + 0.0291(U^*/9.8)^2} \tag{9}$$

Fig. 13 presents the fitted curve of the across-wind aerodynamic damping ratio given by Eq. (9),

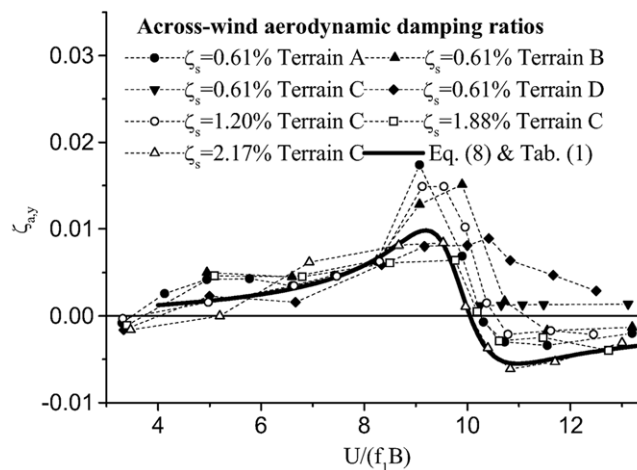


Fig. 13 Comparison of across-wind aerodynamic damping ratios from wind tunnel test with Eq. (9)

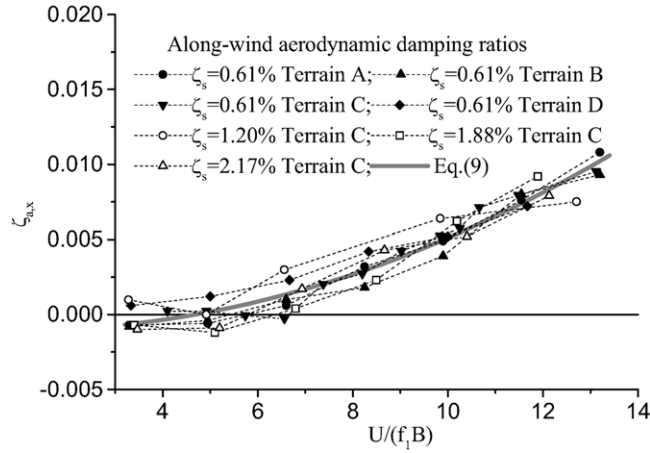


Fig. 14 Comparison of aerodynamic damping ratios in along-wind direction from wind tunnel test with that from Eq. (10)

together with the testing results for comparison. It can be seen from the figure that Eq. (9) is essentially an envelope curve and it approximately takes minimum values for the positive aerodynamic damping ratio range and takes maximum absolute values for the negative aerodynamic damping ratio range. This envelope principle will make structural design of buildings tend to safety and seems to be proper for practical purpose.

The effects of wind field condition and structural damping ratio on the along-wind aerodynamic damping ratios seem to be negligible from practical point of view. Eq. (10) is a formula for along-wind aerodynamic damping ratio which has been fitted also using least square approximation method. Fig. 14 shows the comparison of the test results with Eq. (10). The fitted curve can reflect the testing results well.

$$\zeta_a = 0.000075U^{*2} - 0.00014U^* - 0.001 \quad (10)$$

## 7. Computation of across-wind dynamic responses considering aerodynamic damping

To verify the accuracy of the formulas of the across-wind aerodynamic damping ratio, across-wind dynamic response of a super high-rise square building is calculated by Eq. (8) and Table 1 with power spectrum of across-wind base moment obtained from its high frequency balance wind tunnel test (Ming and Yong 2004, Yong 2002, Yong and Ming 2002), with and without considering the effect of aerodynamic damping ratio and then compared with the corresponding response from the aeroelastic model test.

Generally speaking, when the aerodynamic damping is taken into account, the computed across-wind dynamic responses of the building are closer to the responses from the aeroelastic model test. Fig. 15(a) shows the non-dimensional dynamic displacements of the building with structural damping ratio of 0.61% and located in terrain category A; and Fig. 15(b) presents the results for the condition of structural damping ratio of 1.2% and terrain category C. As can be seen from Fig. 15(a), the maximum dynamic displacement from the computation without considering the effect of

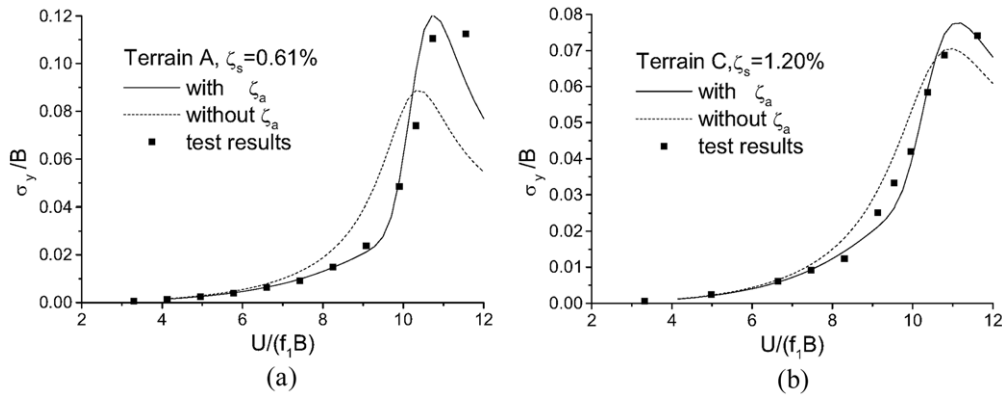


Fig. 15 Comparison of computed RMS displacement by Eq. (8) and Table 1 with aeroelastic model test results for two test cases

aerodynamic damping is only about 75% of that from the aeroelastic model test; while the maximum response considering the effect of aerodynamic damping is almost the same as the corresponding value from the aeroelastic model test. Moreover, Fig. 15(b) indicates that the effect of aerodynamic damping on the across-wind responses is much less for a building that has higher structural damping and is situated in a rougher area. The comparison of Fig. 15(a) and Fig. 15(b) seems to indicate that across-wind aerodynamic damping plays an important role in estimation of across-wind dynamic responses of super high-rise buildings, and the formulas for across-wind aerodynamic damping are precise enough for practical purpose.

## 8. Conclusions

A SDOF aeroelastic model of square super high-rise buildings with an aspect ratio of 6 was tested and its across- and along-wind aerodynamic damping ratios were identified from its random vibration responses in simulated wind field using the Random Decrement technique. The effects of reduced velocity and terrain condition and structural damping ratio on the across- and along-wind aerodynamic damping ratios are investigated in detail. Formulas of across- and along-wind aerodynamic damping ratios are then derived. Accuracy of these formulas is verified through detailed comparisons between the values from the formulas and those from the present test and other literatures. The across-wind dynamic responses of square buildings are finally calculated with the power spectrum of across-wind base moment with and without considering the effect of the aerodynamic damping ratio and then compared with the corresponding responses from the aeroelastic model test. The comparison results show that the across-wind aerodynamic damping may play an important role in estimation of across-wind dynamic response of super high-rise buildings, and the formulas for across-wind aerodynamic damping are precise enough for practical purpose.

## Acknowledgements

This project was jointly supported by Chinese National Natural Science Foundation (50321003) and Ministry of Education, Culture, Sports, Science and Technology, Japan, through the 21st Century Center of Excellence Program, which are gratefully acknowledged.

## References

- Chinese Code for Loading on Buildings and other Structures, GB50009-2001, 2001 (in Chinese).
- Glanville, M.J., Kwok, K.C.S. and Denoon, R.O. (1996), "Full-scale measurements of structures in Australia", *J. Wind Eng. Ind. Aerodyn.*, **59**, 349-364.
- Huang, P. (1997), "Simulation of the wind fields of the atmospheric boundary layer and the peak factors of fluctuating pressure of high-rise buildings", Thesis for the degree of Master, Tongji University, Shanghai, China.
- Jeary, A.P. (1996), "The description and measurement of nonlinear damping in structures", *J. Wind Eng. Ind. Aerodyn.*, **59**, 103-114.
- Kareem, A. (1978), "Wind excited motion of buildings", Ph. D. Thesis, Colorado State University at Fort Collin, Colorado.
- Kareem, A. and Gurley, K. (1996), "Damping in structures: its evaluation and treatment of uncertainty", *J. Wind Eng. Ind. Aerodyn.*, **59**, 131-157.
- Marukawa, H., Kato, N., Fujii, K. and Tamura, Y. (1996), "Experimental evaluation of aerodynamic damping of tall buildings", *J. Wind Eng. Ind. Aerodyn.*, **59**, 177-190.
- Ming, G. and Yong, Q. (2004), "Across-wind aerodynamic force of typical tall buildings", *J. Wind Eng. Ind. Aerodyn.*, **92**, Issue **13**, 1147-1165.
- Nishimura, H. and Taniike, Y. (1995), "Unsteady wind force on a square prism in a turbulent boundary layer", *9ICWE*, New Delhi, India, 195-203.
- Steckley, A. (1989), "Motion-induced wind forces on chimneys and tall buildings", Ph.D. Thesis, University of Western Ontario.
- Tamura, Y. and Suganuma, S.Y. (1996), "Evaluation of amplitude-dependent damping and natural frequency for buildings during strong winds", *J. Wind Eng. Ind. Aerodyn.*, **59**, 115-130.
- Tamura, Y., Suda, K. and Sasaki, A. (2000), "Damping in buildings for wind resistant design", *International Symposium on Wind and Structures for the 21st Century 26-28 January*, Cheju, Korea, 115-129.
- Watanabe, Y., Isyumov, N. and Davenport, A.G. (1997), "Empirical aerodynamic damping function for tall building", *J. Wind Eng. Ind. Aerodyn.*, **72**, 313-321.
- Yong, Q. (2002), "The across-wind loads and responses of super high-rise buildings", Ph.D. thesis, Tongji University, Shanghai, China (in Chinese).
- Yong, Q. and Ming, G. (2002), "The across-wind aerodynamic force spectra of super high-rise buildings", *Journal of Tongji University*, **30**(5), 627-632 (in Chinese).